NUCL SCI TECH (2018) 29:175
https://doi.org/10.1007/s41365-018-0512-z

Nonlinear energy chirp compensation with corrugated structures

Zhen Wang[1] · Chao Feng[1] · Da-Zhang Huang[1] · Qiang Gu[1] · Meng Zhang[1]

Received: 17 July 2018 / Revised: 19 September 2018 / Accepted: 19 September 2018 / Published online: 16 November 2018

Abstract Herein, a feasible method is proposed to compensate the high-order effect during bunch length compression, thereby enhancing the peak current of a high-repetition-rate X-ray free-electron laser source. In the proposed method, the corrugated structure is inserted downstream of the high-order harmonic cavities to function as a passive linearizer and enhance the longitudinal profile of the electron beam. Three-dimensional simulations are performed to analyze the evolution of the longitudinal phase space, and the results demonstrate that the profile of the electron beam is improved and the peak current can be easily optimized to over 2 kA with a bunch charge of 100 pC.

Keywords Corrugated structure · Nonlinear energy chirp · High-repetition-rate FEL

1 Introduction

Unlike conventional lasers or synchrotron radiations, a free-electron laser (FEL) can generate ultra-short, ultra-bright, and fully coherent hard X-ray radiations, which is at the origin of FELs extensive development over the last decade [1, 2]. Nowadays, many X-ray FEL facilities exist or are under-construction around the world, such as LCLS in the USA [3], SACLA in Japan [4], FERMI in Italy [5, 6], Pal-FEL in Korea [7], SXFEL in China [8–12], and Swiss-FEL in Switzerland [13]. As these facilities are driven by the common conducting (copper) linear accelerator (linac), their repetition rates are in the range of 1–120 Hz, leading to a relatively low average power.

Alternatively, high-repetition-rate FEL facilities based on superconducting (SC) techniques have been studied for years. For example, FLASH in Germany [14], a soft X-ray user facility based on macro-bunch modes, has accumulated extensive experience on SC techniques. Recently, the European XFEL [15] successfully generated hard X-ray FEL, which is a milestone in the FEL community. LCLS II based in the USA and SHINE in China [16], which have been recently launched, are hard X-ray FEL facilities based on SC linac with continuous-wave (CW) modes. These high-repetition-rate (about 1 MHz) FEL facilities could provide up to a 1000-fold increase in average brightness compared with the common conducting FEL facilities.

In order to provide the CW electron beam train, the common conducting very-high-frequency (VHF) gun [17–19], the high-voltage direct current (DC) gun [20], or the SC RF gun [21] are developed as the injector of the CW FEL facilities. As the beam energy from these guns is relatively low compared with that of the usual conducting copper photocathode gun, the high-order terms of the electron longitudinal phase space play an important role in the forthcoming electron beam compression process, suffering from strong space charge effects. The peak current of the electron beam at the exit of the SC linac is limited to approximately 1 kA, which is much lower than that of the common conducting linac. This usually leads to a

This work was supported by the National Natural Science Foundation of China (Nos. 11675248 and 11775294) and the Youth Innovation Promotion Association CAS (No. 2018300).

✉ Meng Zhang
zhangmeng@sinap.ac.cn

[1] Shanghai Institute of Applied Physics, Chinese Academy of Sciences, Shanghai 201800, China

degradation of the FEL performance, more particularly for FEL lasing in hard X-ray regime.

Herein, the use of corrugated structures is proposed to compensate for the high-order terms during the compression process, as these structures are usually employed as a beam energy dechirper [22–25]. These corrugated structures are inserted upstream of the first bunch compressor chicane, providing a passive wakefield to modulate the longitudinal phase space of the electron beam. Three-dimensional start-to-end simulations are performed to study the evolution of the longitudinal phase space, and the results with and without the corrugated pipe are compared. The results demonstrated that the longitudinal phase space is improved and the peak current of the electron beam at the exit of the SC linac can be enhanced to over 2 kA.

The principle of the compression process and the basic analytic properties of the corrugated pipe are introduced in section II of this manuscript. The start-to-end simulation studies are performed with an optimized corrugated pipe for SHINE in section III. Finally, a summary and conclusions are briefly stated in section IV.

2 Theory

In the case of the usual conducting hard X-ray FEL facilities, the nonlinear effects, such as the sinusoidal RF time curvature and the second-order momentum compaction terms during the compression process, dominate the final peak current of the electron beam. A harmonic cavity, usually an X-band, is used to linearize the bunch compression process and compensate for the second-order compression effects [20]. Similarly, a third harmonic cavity is used as the linearizer upstream of the first bunch compressor chicane (BC1) in the SC linac-based high-repetition-rate FEL facilities. The schematic layout of the gun, the linac segments, and the first chicane is presented in Fig. 1, with the symbols defined as the voltage (V), the RF phase (ϕ), the wavelength (λ) of each cryomodule in the injector (L0 CM) and the linac (L1 CM), and the chicane momentum compaction coefficients (R_{56}, T_{566}).

Based on the analysis for a high-harmonic cavity [26], the necessary harmonic voltage as can be calculated as follows:

$$eV_3\cos\phi_3 = \frac{E_0\left[1-\frac{\lambda_1^2}{2\pi^2}\frac{T_{566}}{R_{56}^3}\left(1-\frac{\sigma_z}{\sigma_{z_0}}\right)^2\right]-E_i}{1-\left(\frac{\lambda_1}{\lambda_3}\right)^2}, \quad (1)$$

where E and σ are the energy and the duration of the electron beam at different locations of the beamline, respectively.

However, suffering from the strong space charge effect in the injector, the compression process is dominated by the higher-order terms of the energy chirp. The typical longitudinal phase space of the electron beam at the end of the SC linac is presented in Fig. 2. It can be seen that the bunch-length-scale energy modulation leads to a double-horn density distribution and the current in the high-quality central part of the electron beam is approximately 1 kA.

In order to improve the peak current of the electron beam, thus the FEL performance, the high-order terms must be compensated during the compression process. The corrugated structure, having a near-maximal possible amplitude for a given aperture, is an attractive solution to compensate for the high-order terms of the energy chirp as the "additional linearizer" [27]. The geometry of the corrugated structure is presented in Fig. 3. A relativistic electron beam passing on-axis through a periodic-corrugated cylindrical pipe with the radius of a is considered. The corrugated gap is represented as g, the period as p, and the depth as δ, with $\delta, p \ll a$. At the same time, a "steeply corrugated" structure is assumed, requiring $\delta \geq p$.

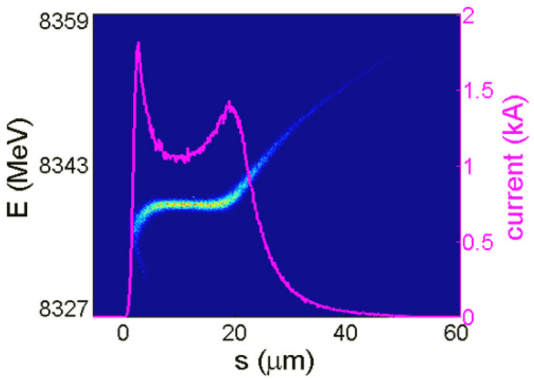

Fig. 2 (Color online) Longitudinal phase space of the electron beam at the exit of the linac. The bunch head is represented on the left. s is the coordinate along the beam

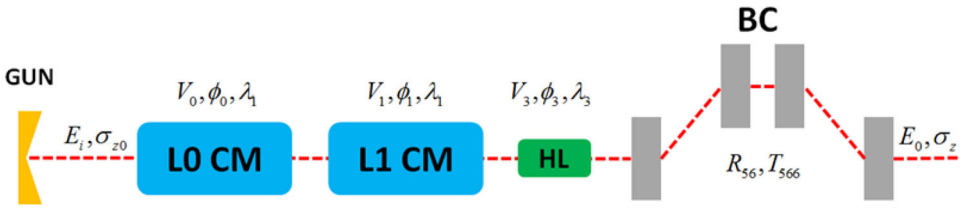

Fig. 1 (Color online) Schematic layout of the gun, the linac segments, and the first chicane. The voltages and the phases in L0 CM are defined as the equivalent values V_0 and ϕ_0 for simplicity

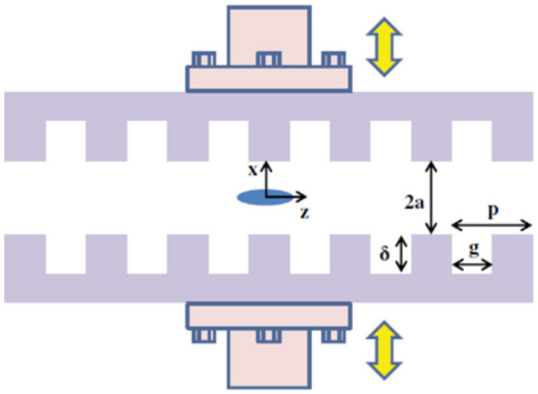

Fig. 3 (Color online) The geometry of the corrugated structure

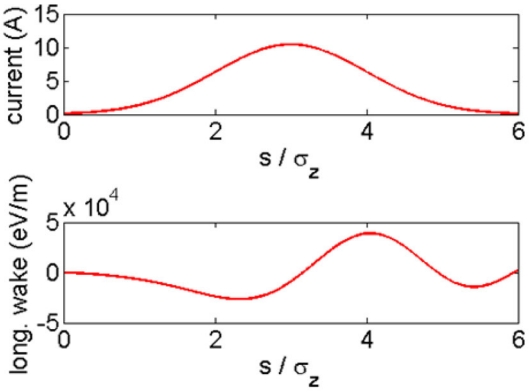

Fig. 4 The Gaussian bunch and the longitudinal wake along the bunch

When the relativistic charged beam passes through the structure, the longitudinal point charge wake is approximately expressed as [22–25, 27]:

$$W(s) = 2\chi H(s)\cos ks, \tag{2}$$

where χ is the mode loss factor.

$$\chi = \frac{Z_0 c}{2\pi a^2}, \tag{3}$$

where $Z_0 = 377\ \Omega$ represents the characteristic impedance of vacuum and c is the speed of light. $H(s)$ is the unit step function defined as:

$$H(s) = \begin{cases} 1, & s \geq 0 \\ 0, & s < 0 \end{cases}, \tag{4}$$

and the wave number, k, is approximated defined as:

$$k = \sqrt{\frac{2p}{a\delta g}}. \tag{5}$$

For a bunch with longitudinal distribution $\lambda(s)$, the bunch wake is defined by the convolution:

$$W_\lambda(s) = -\int_0^{+\infty} W(s')\lambda(s - s')\mathrm{d}s', \tag{6}$$

considering a Gaussian bunch density distribution beam with a bunch length of σ_z without any current fluctuation. By changing the geometry parameters of the corrugated structure, as presented in Fig. 3, thus optimizing the wavelength of the induced energy modulation, the high-order energy chirp of the electron beam can be compensated and the peak current can be improved. It should be noted that, to optimize the parameters of the corrugated structure, the wavelength of the main high-order terms of the bunch energy chirp should be analyzed. Therefore, the proper wavelength of the bunch wake (equal to the wavelength of the high-order terms) can be determined with Eq. (6). For the electron beam in SHINE, the wavelength of the point charge wake is approximately equal to the bunch length. The induced wakefield within the beam is represented in Fig. 4, where the quasiperiodic energy modulation along the beam introduced by the wakefield can be observed.

3 Nonlinear effect compensation for the SHINE project

The SHINE will be the first hard X-ray FEL user facility based on the SC technique in China. The injector consists of a normal conducting electron RF gun (the VHF gun), a 1.3 GHz buncher, an eight 9-cell 1.3 GHz TESLA-like cryomodule (CM) [28], and a laser heater, providing an initial electron beam having a length of approximately 10 ps in full width at half maximum (FWHM), charge of 100 pC, peak current of about 10 A, and bunch rate up to 1 MHz. The main linac consists of three sections: L1 (two CMs with a beam energy of approximately 250 MeV), L2 (18 CMs, 2.1 GeV), and L3 (54 CMs, over 8 GeV), two bunch compressor chicanes BC1 (compressing the beam current from 10 to 80 A) and BC2 (80 A to 1 kA), and a dechirper line at the end of the linac to compensate the correlated energy spread. Moreover, a 3.9 GHz third harmonic structure is located in L1 acting as a linearizer (harmonic linearizer, HL) to provide extra energy chirp and compensate for the second-order compression effects. The electron beam, after being generated in the injector and accelerated in the linac, with a bunch length of 8 μm in FWHM and a peak current of 1 kA, is finally sent to the downstream switchyard and the undulator systems for X-ray FEL generations. The layout of the injector and the linac of the SHINE is presented in Fig. 5. The main beam parameters of the SHINE are listed in Table 1.

In order to illustrate the beam dynamic of the bunch, three-dimensional simulations are performed with all

Fig. 5 (Color online) Layout of the injector and the linac of SHINE

Table 1 Main beam parameters of the SHINE

Parameters	Values
Energy (GeV)	8
Slice energy spread (rms)	$\leq 0.01\%$
Normalized slice emittance (mm mrad)	≤ 0.4
Charge (pC)	100
Repetition rate (MHz)	≤ 1
Peak current (kA)	1
Bunch length (rms) (μm)	8
Transverse beam size (rms) (μm)	30

beamline components. The injector simulations are accomplished using the computer tracking codes ASTRA [29] considering the space charge effects. The main linac simulations are performed using ELEGANT [30], in which the coherent synchrotron radiation and the wakefield effects are considered. The longitudinal phase space evolution of the electron beam along the beamline is presented in Fig. 6. The peak current of the high-quality part of the electron beam is only of approximately 1 kA, and the double-horn-like current distribution limits the higher peak current due to the high-order terms of beam energy chirp.

On the other hand, the bunch length is relatively long in the gun (approximately 30 ps) and the injector (approximately 10 ps after the buncher). This is comparable to the wavelength of the wakefield excited by the beam itself. As described above, the field along the bunch is no longer linear (as observed in Fig. 4). By optimizing the parameters of the corrugated structure, the wavelength and the energy distribution of the structure-induced wakefield based on the given density distribution of the electron beam

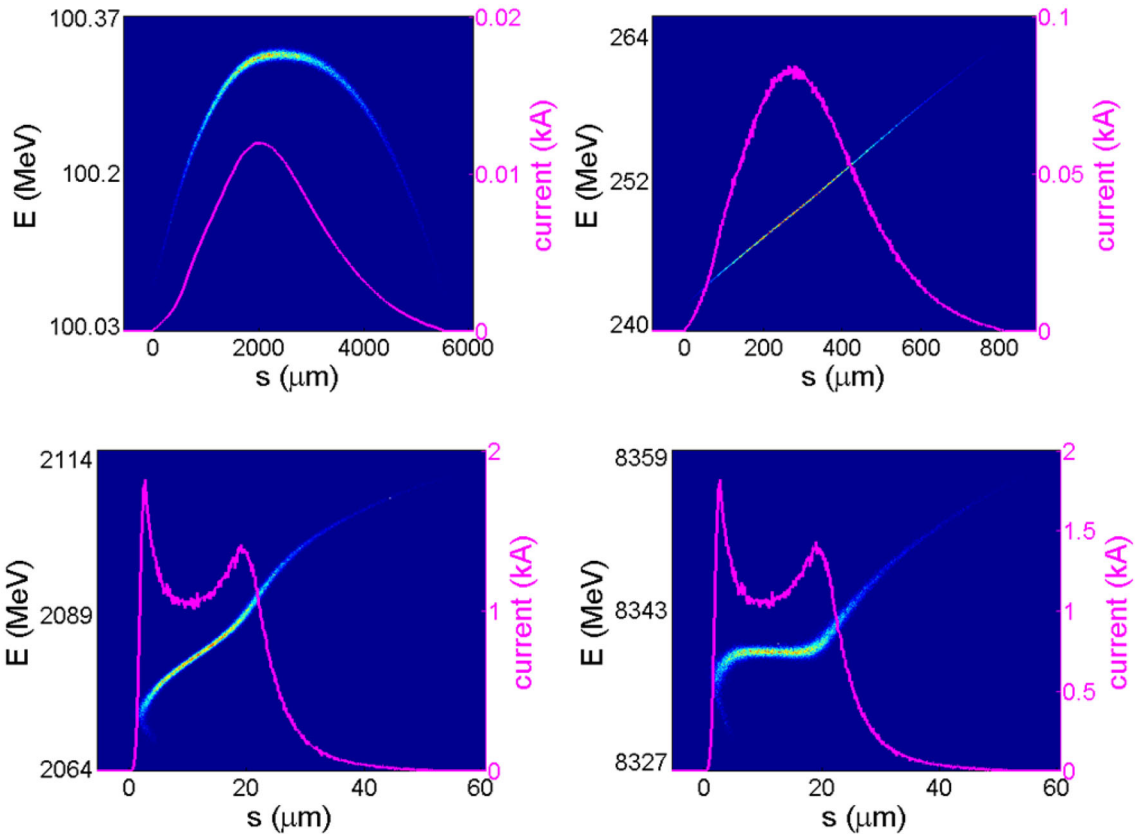

Fig. 6 (Color online) Longitudinal phase space evolution along the beamline at the exit of (top left) the injector, (top right) the BC1, (bottom left) the BC2, and (bottom right) the linac

Table 2 Main parameters of the corrugated structure

Parameters	Values
Radius, a (mm)	2.5
Period, p (mm)	1.0
Depth, δ (mm)	0.4
Width, g (mm)	0.2
Length, L (m)	0.4

can be adjusted, and this can be used to compensate for the high-order energy chirp. In order to operate these adjustments, simulations (with LiTrack for 2D and ELEGANT for 3D) are performed to analyze the longitudinal phase space evolution of the electron beam based on the SHINE linac layout and are presented in Fig. 6. By plotting the central energy distribution of the electron beam at the exit of BC2 after removal of the linear correlation of energy chirp, the modulation period and amplitude can be calculated. Multiplied by the compression ratio, the modulation period before bunch compressor can be deducted. In order to compensate for the modulation, the gap and the length of corrugated structure can be scanned to adjust the modulation wavelength and amplitude based on the given Gaussian-like current distribution electron beam in the injector. Herein, the compression ratio is approximately 100 and the modulation period is approximately 3 mm. A 0.4-m-long corrugated pipe following the parameters in Table 2 is inserted downstream of the 3.9 GHz third harmonic cavities in the L1 section in order to compensate for the high-order terms of energy chirp. The longitudinal phase space evolution of the electron beam along the linac is shown in Fig. 7. The double-horn density distribution disappears, and the final current distribution is Gaussian-like with a peak current of approximately 1 kA. Compared with Fig. 6, a distinct improvement in the linearity mainly can be observed in BC2 due to the high-order terms of energy chirp playing a more important role when the compression ratio is higher.

Furthermore, the accelerating phases and the compaction coefficients (R_{56} and T_{566}) of BC1 and BC2 can be optimized to compress the beam to higher peak current, and this is even more critical for FEL operations in a hard X-ray regime. The longitudinal phase space, beam current, and slice energy spread distribution at the exit of the linac are summarized in Fig. 8. The beam current can be easily enhanced to over 2 kA in an approximately 50 fs wide region. The beam quality has been maintained in this region, where the slice energy spread is approximately

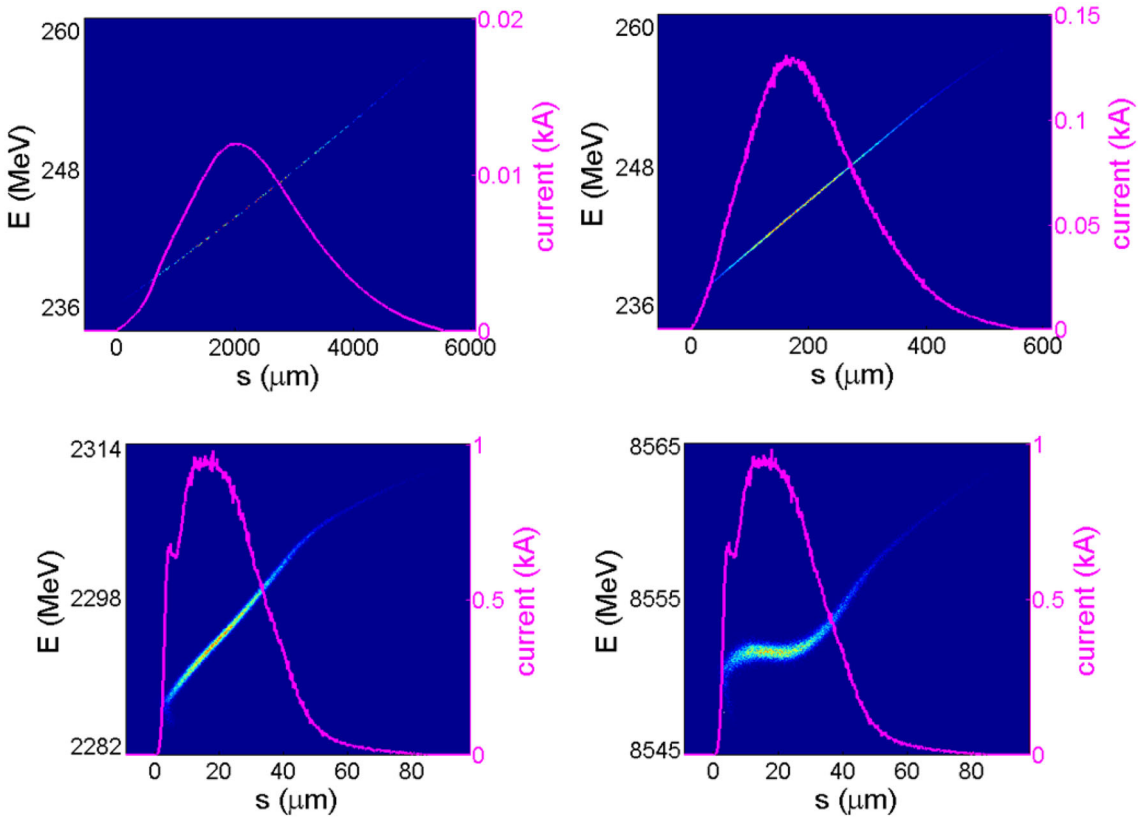

Fig. 7 (Color online) Longitudinal phase space of the electron beam at the exit of (top left) the corrugated pipe, (top right) the BC1, (bottom left) the BC2, and (bottom right) the linac with the corrugated pipe as the additional linearizer

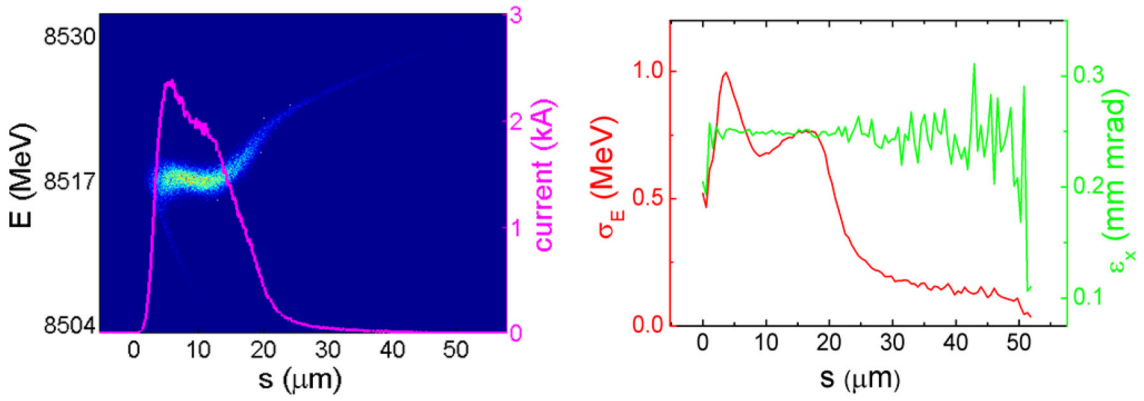

Fig. 8 (Color online) (left) Longitudinal phase space of the electron beam, (right) slice energy spread, and normalized slice emittance distribution along the beam

800 keV and the normalized slice emittance is approximately 0.25 mm mrad.

4 Conclusion

Due to nonlinear space charge effects, the peak current of the electron beam is limited to approximately 1 kA in high-repetition-rate free-electron laser light source. In order to improve the peak current, the corrugated structure was proposed to be employed as an "additional linearizer" downstream of the third harmonic cavity to compensate for the high-order terms of energy chirp during the compression process. The optimal parameters of the corrugated structures were determined, and the simulation results demonstrated that this novel scheme is feasible. The double-horn current distribution was suppressed and the current distribution profile was optimized based on the SHINE beam. In addition, the beam was compressed further to higher peak current, e.g., over 2 kA according to our simulations, which will significantly improve the performance of a SC-linac-based FEL.

Acknowledgements The authors thank Prof. Hai-Xiao Deng, Duan Gu, and Zhen-Tang Zhao for the useful discussions.

References

1. J.M.J. Madey, Stimulated emission of bremsstrahlung in a periodic magnetic field. J. Appl. Phys. **42**, 1906 (1971). https://doi.org/10.1063/1.1660466
2. C. Feng, H.X. Deng, Review of fully coherent free-electron laser. Nucl. Sci. Tech. **29**, 160 (2018). https://doi.org/10.1007/s41365-018-0490-1
3. P. Emma, R. Akre, J. Arthur et al., First lasing and operation of an ångstrom-wavelength free-electron laser. Nat. Photonics **4**, 641 (2010). https://doi.org/10.1038/nphoton.2010.176
4. H. Tanaka, H. Aoyagi, T. Asaka et al., A compact X-ray free-electron laser emitting in the sub-ångstrom region. Nat. Photonics **6**, 540 (2012). https://doi.org/10.1038/nphoton.2012.141
5. E. Allaria, R. Appio, L. Badano et al., Highly coherent and stable pulses from the FERMI seeded free-electron laser in the extreme ultraviolet. Nat. Photonics **6**, 699 (2012). https://doi.org/10.1038/nphoton.2012.233
6. E. Allaria, D. Castronovo, P. Cinquegrana et al., Two-stage seeded soft-X-ray free-electron laser. Nat. Photonics **7**, 913 (2013). https://doi.org/10.1038/nphoton.2013.277
7. H. Kang, C. Min, H. Heo et al., Hard X-ray free-electron laser with femtosecond-scale timing jitter. Nat. Photonics **11**, 708 (2017). https://doi.org/10.1038/s41566-017-0029-8
8. Z.T. Zhao, Shanghai soft x-ray free electron laser test facility, in *Proceedings of IPAC2011, San Sebastián, Spain, THPC053*
9. Z. Wang, C. Feng, Q. Gu et al., Generation of double pulses at the Shanghai soft X-ray free electron laser facility. Nucl. Sci. Tech. **28**, 28 (2017). https://doi.org/10.1007/s41365-017-0188-9
10. M. Song, C. Feng, D. Huang et al., Wakefields studies for the SXFEL user facility. Nucl. Sci. Tech. **28**, 90 (2017). https://doi.org/10.1007/s41365-017-0242-7
11. Q. Yu, D. Gu, M. Zhang et al., Transverse phase space reconstruction study in Shanghai soft X-ray FEL facility. Nucl. Sci. Tech. **29**, 9 (2018). https://doi.org/10.1007/s41365-017-0338-0
12. Y. Bian, W. Zhang, B. Liu et al., Sub-picosecond electron bunch length measurement using coherent transition radiation at SXFEL. Nucl. Sci. Tech. **29**, 74 (2018). https://doi.org/10.1007/s41365-018-0399-8
13. B.D. Patterson, R. Abela, H. Braun et al., Coherent science at the SwissFEL x-ray laser. New J. Phys. **12**, 035012 (2010). https://doi.org/10.1088/1367-2630/12/3/035012
14. W.A. Ackermann, G. Asova, V. Ayvazyan et al., Operation of a free-electron laser from the extreme ultraviolet to the water window. Nat. Photonics **1**, 336 (2007). https://doi.org/10.1038/nphoton.2007.76
15. M. Altarelli, R. Brinkmann, M. Chergui et al., XFEL: The European X-Ray Free-Electron Laser—Technical Design Report (DESY, Ham-burg, 2006), pp. 1–646
16. Z.T. Zhao, C. Feng, K. Zhang, Two-stage EEHG for coherent hard X-ray generation based on a superconducting linac. Nucl. Sci. Tech. **28**, 117 (2017). https://doi.org/10.1007/s41365-017-0258-z
17. A. Opanasenko, V. Mytrochenko, V. Zhaunerchyk et al., Design study of a low-emittance high-repetition rate thermionic rf gun. Phys. Rev. Accel. Beams **20**, 053401 (2017). https://doi.org/10.1103/PhysRevAccelBeams.20.053401

18. Z. Ding, S. Karkare, J. Feng et al., Temperature-dependent quantum efficiency degradation of K-Cs-Sb bialkali antimonide photocathodes grown by a triple-element code position method. Phys. Rev. Accel. Beams **20**, 113401 (2017). https://doi.org/10.1103/PhysRevAccelBeams.20.113401
19. R. Huang, D. Filippetto, C. Papadopoulos et al., Dark current studies on a normal-conducting high-brightness very-high-frequency electron gun operating in continuous wave mode. Phys. Rev. Accel. Beams **18**, 013401 (2015). https://doi.org/10.1103/PhysRevSTAB.18.013401
20. C. Gulliford, A. Bartnik, I. Bazarov et al., Demonstration of low emittance in the Cornell energy recovery linac injector prototype. Phys. Rev. Accel. Beams **16**, 073401 (2013). https://doi.org/10.1103/PhysRevSTAB.16.073401
21. T. Rao, I. Ben-zvi, A. Burrill et al., Design, construction and performance of all niobium superconducting radio frequency electron gun. Nucl. Instrum. Methods Phys. Res. Sect. A **562**, 22–33 (2006). https://doi.org/10.1016/j.nima.2006.02.172
22. K.L.F. Bane, G. Stupakov, Impedance of a rectangular beam tube with small corrugations. Phys. Rev. Spec. Top. Accel. Beams **6**, 024401 (2003). https://doi.org/10.1103/PhysRevSTAB.6.024401
23. K.L.F. Bane, G. Stupakov, Corrugated pipe as a beam dechirper. Nucl. Instrum. Methods Phys. Res. Sect. A **690**, 106–110 (2012). https://doi.org/10.1016/j.nima.2012.07.001
24. K.L.F. Bane, G. Stupakov, Dechirper wakefields for short bunches. Nucl. Instrum. Methods Phys. Res. Sect. A **820**, 156–163 (2016). https://doi.org/10.1016/j.nima.2016.02.055
25. K. Bane, G. Stupakov, I. Zagorodnov, Analytical formulas for short bunch wakes in a flat dechirper. Phys. Rev. Accel. Beams **19**, 084401 (2016). https://doi.org/10.1103/PhysRevAccelBeams.19.084401
26. P. Emma, X-band RF harmonic compensation for linear bunch compression in the LCLS, SLAC-TN-05-004, LCLS-TN-01-1, November 14, 2001
27. Q. Gu, M. Zhang, M.H. Zhao, A passive linearizer for bunch compression, in *Proceedings of LINAC2012, Tel-Aviv, Israel TUPB022*
28. B. Aune, R. Bandelmann, D. Bloess et al., Superconducting TESLA cavities. Phys. Rev. Spec. Top. Accel. Beams **3**, 092001 (2000). https://doi.org/10.1103/PhysRevSTAB.3.092001
29. K. Floettmann, ASTRA user's manual. http://www.desy.de/mpyflo/Astra_dokumentationS. Accessed 13 Nov 2018
30. M. Borland, Elegant: a flexible SDDS-compliant code for accelerator simulation. Advanced Photon Source Report No. LS-287, 2000